Nanoscale

ROYAL SOCIETY OF CHEMISTRY

PAPER

View Article Online
View Journal | View Issue

Cite this: *Nanoscale*, 2020, **12**, 8397

Resonant scattering-enhanced photothermal microscopy†

Qiang Li, [a] Zhonghong Shi,[a] Lijun Wu*[a] and Hong Wei *[b,c]

Photothermal (PT) microscopy is currently the most efficient approach for the detection and spectroscopy of individual non-fluorescent nano-objects based solely on their absorption. The nano-objects in current PT microscopy are usually non-resonant with the probe laser light, and the PT signal is mainly generated from the interactions of the incident probe light and the heating light-induced thermal lens around the imaged object. Inspired by the high sensitivity of the scattering field from the nano-objects near optical resonance to the variation in the local refractive index, we developed a novel strategy of resonant scattering-enhanced PT microscopy where the imaged nano-objects are near-resonant with the probe laser light. We have demonstrated this by using gold nanorods (NRs) with tunable longitudinal surface plasmon resonances. The PT signal of gold NR near-resonant with the probe light showed dramatic variation in the narrow resonance wavelength range, as small as 15 nm, and the maximal amplitude of the PT signal in this range can be enhanced up to 43 times as compared with the weak PT signal of gold NR non-resonant with the probe light. Theoretical analysis indicates that the obtained strong PT signal is mainly caused by the heat-induced variation in the polarizability of gold NR. Our novel work demonstrates the first resonant scattering-enhanced PT imaging of plasmonic nanoparticles, paving the way for the development of PT microscopy with ultra-high sensitivity toward the sensing, imaging, and spectroscopy of nanoscopic objects in complex environments.

Received 27th December 2019,
Accepted 18th March 2020

DOI: 10.1039/c9nr10893a

rsc.li/nanoscale

Introduction

In contrast to fluorescence and scattering-based optical detection approaches,[1–8] absorption-based photothermal (PT) microscopy does not suffer from photobleaching and photoblinking,[9–11] and it is insensitive to the presence of non-absorbing large objects that predominantly scatter,[12–15] making it attractive for the robust detection of absorbing nanoparticles. In typical PT microscopy, the imaged nanoparticles are usually resonantly excited by an intensity-modulated heating beam. The excitation energy can be non-radiatively dissipated as heat into the local environment, establishing localized temperature variation around each nanoparticle. Because of the thermo-optic effect, local refractive index perturbation, also called thermal lens (TL), is created.[16] The dielectric TL around the imaged nanoparticle can be measured by the phase-sensitive, heterodyne detection of the transmitted or reflected field of a probe laser beam. In this technique, the room temperature detection of small gold nanoparticles,[17–22] individual quantum dots,[23] single carbon nanotubes,[24,25] and even single non-fluorescent molecules[26] has been demonstrated.

In the current PT microscopy, the imaged nanoparticles are usually non-resonant with the probe laser light, and the PT signal is mainly generated from the interaction of the probe light and TL. Because the thermo-optic coefficient is usually quite small,[14] the change in the probe beam intensity is extremely weak and difficult to detect. As such, the high power of the heating beam (increasing the rise in the local temperature) and probe beam (reducing the photon noise) and the long integration time of the lock-in amplifier are usually required in order to obtain an acceptable signal to noise ratio. This can cause serious limitations for biological applications, especially for live-cell imaging, because the strong and long-time laser light stimulation could denature biological molecules and alter cellular functions. Therefore, improving the signal to noise ratio of PT microscopy under weak laser light conditions is critical for its further biological applications. The interaction of probe light and dielectric TL shows little wavelength dependence, so it is difficult to develop multicolor PT microscopy without employing wavelength-dependent absorp-

[a]*Guangdong Provincial Key Laboratory of Nanophotonic Functional Materials and Devices, School of Information and Optoelectronic Science and Engineering, South China Normal University, Guangzhou 510006, China. E-mail: ljwu@scnu.edu.cn*
[b]*Institute of Physics, Chinese Academy of Sciences, Beijing 100190, China. E-mail: weihong@iphy.ac.cn*
[c]*Songshan Lake Materials Laboratory, Dongguan 523808, China*
†Electronic supplementary information (ESI) available. See DOI: 10.1039/c9nr10893a

tion.[21] Compared with the nanoparticles far away from the optical resonance, the scattering and absorption of nanoparticles in near-resonance are very sensitive to variations in the local environment, which play an important role in the field of optical detection and sensing.[27,28] Herein, we demonstrate that the high sensitivity of the scattering field from nanoparticles near-resonant with the probe light to the variation in the local temperature can largely enhance the signal to noise ratio of PT microscopy.

Experimental section

The sample for resonant scattering-enhanced PT imaging simply consisted of chemically synthesized gold NRs placed on top of a glass substrate. In order to enhance the PT effect of the gold NR, polyvinyl alcohol (PVA) film, with a high thermo-optic coefficient and low thermal conductivity, was spin-coated as the embedding medium of the gold NR (see section 1 and 2 of ESI† for more details). The gold NRs are efficient point heat sources upon heating light illumination. The diameters of the gold NRs were about 20 nm and their lengths were distributed in the range of 30 nm to 70 nm. Fig. 1a presents the general elements of the PT microscope. After passing through the acousto-optic modulator (AOM) with a typical modulation frequency of 80 kHz, the circularly polarized heating laser beam of 532 nm wavelength was overlaid with the linearly polarized probe beam of 730 nm wavelength. The two collimated beams were focused onto the same spot on the sample surface through a 100× oil immersion objective with a numerical aperture (NA) of 0.9. The probe light incident on the gold NR generated the interferometric scattering (iSCAT) signal, which is the intensity of the interference field between the scattering light from the gold NR and the reference light reflected at the sample interface (Fig. 1b). The recorded PT signal δ in the experiment is the variation in the iSCAT signal of the gold NR induced by the heat produced by the heating laser beam, that is, $\delta = I'_{iSCAT} - I_{iSCAT}$, where I'_{iSCAT} and I_{iSCAT} are the intensities of iSCAT light measured at the position of the gold NR with and without the heating beam, respectively. The PT signal was obtained using a lock-in amplifier that was in phase referenced to the frequency of AOM. The PT image was recorded by scanning the sample over the fixed laser spots with a step size of 41 nm. The incident power of the heating beam and probe beam was 0.72 mW and 3 μW, respectively. The rise in the local temperature induced by the probe beam was negligible (see section 3 of ESI†).

Results and discussion

Fig. 2a and b show the dark field and the corresponding PT images of several randomly distributed gold NRs on a glass substrate. The PVA film is 50 nm in thickness and the polarization angle θ of the probe light is 140°. Each spot in the PT image corresponds to an individual gold NR. The gold NRs in the PT image can be divided into two categories according to the sign of their PT signal. The positive and negative PT signals mean that the illumination of the heating laser light, *i.e.*, the rise in the local temperature around the imaged gold NR, results in the increased and decreased intensity of the iSCAT light, respectively.

Fig. 2c provides the dark-field scattering spectra of five gold NRs marked as NR1, NR2, NR3, NR4 and NR5 in Fig. 2b. Single Lorentzian line shapes of the five scattering spectra confirmed that these are five single gold NRs. Because of the difference in the aspect ratios of the gold NRs, the peak positions of the measured scattering spectra, *i.e.*, the longitudinal surface plasmon resonance wavelengths λ_{res}, were broadly distributed in the range of 693–755 nm. Importantly, we found

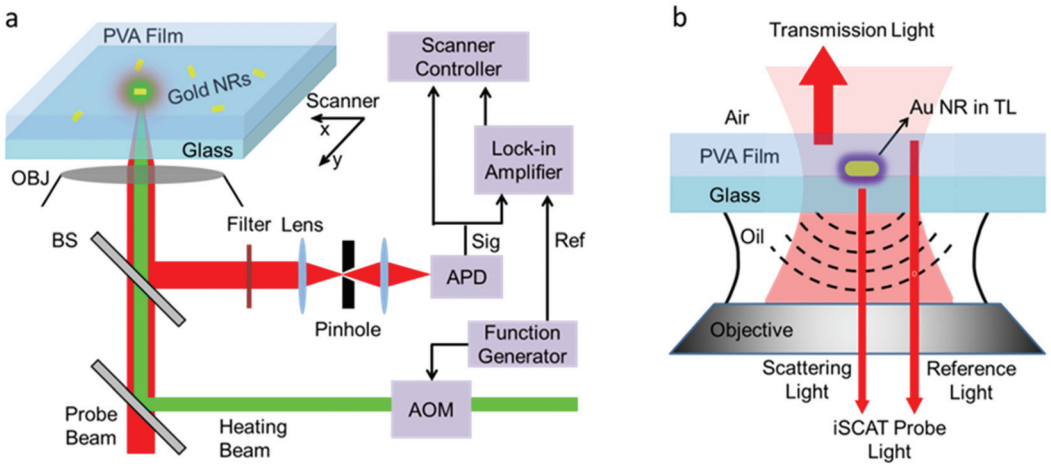

Fig. 1 (a) Scheme of the sample and the PT imaging setup. OBJ, BS, AOM, and APD represent oil objective, beam splitter, acousto-optic modulator, and avalanche photodiode, respectively. "Sig" and "Ref" refer to the voltage signal from the APD and function generator, respectively. The quarter-wave and half-wave plates are not shown in the scheme. (b) Scheme of the iSCAT probe light, which includes the reference light reflected at the sample interface and the scattering light from the gold NR in TL created by the heating beam.

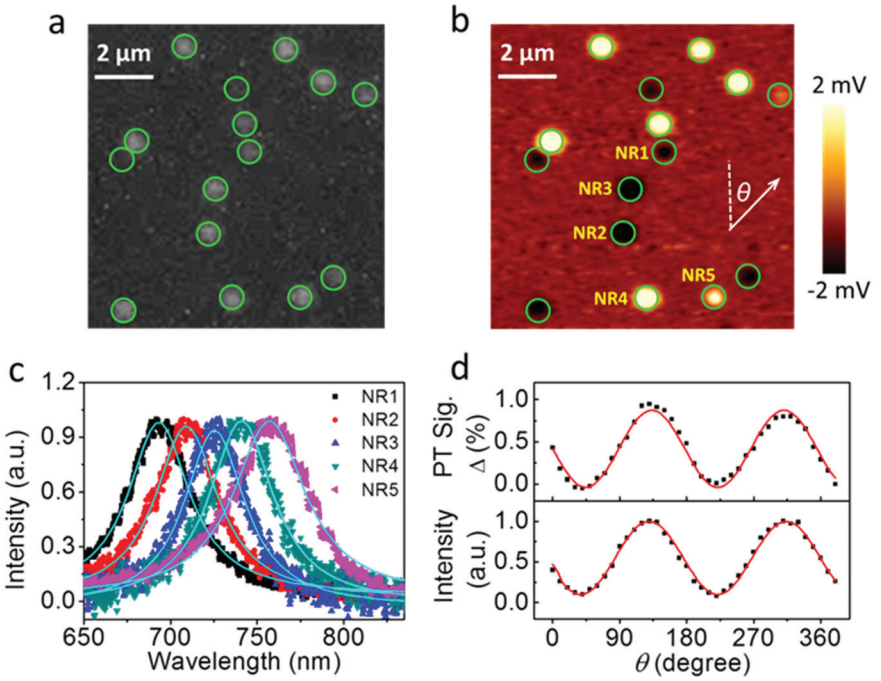

Fig. 2 (a and b) The dark field image (a) and the corresponding PT image (b) of 15 randomly distributed gold NRs on a glass substrate. The PVA film is 50 nm thick. The polarization angle θ of the probe laser light is 140°. The green circles are plotted to mark the positions of the gold NRs. (c) The normalized scattering spectra of the five gold NRs marked as NR1, NR2, NR3, NR4, and NR5 in (b), excited with unpolarized white light and no analyzer in the detection path. Solid lines are Lorentzian fits. The fitted peak positions (widths) of the five gold NRs are 693 (42.8), 709 (43.7), 725 (42.5), 742 (44.8) and 755 (50.3) nm, respectively. (d) The top panel shows the variation in the normalized PT signal Δ of NR4 upon adjusting the polarization angle θ of the probe laser light. The bottom panel shows the peak intensities of the scattering spectra of NR4 as a function of the analyzer angle θ in the detection path. The solid lines are fits of a squared cosine plus offset.

that the resonance wavelengths λ_{res} of gold NRs with positive PT signal (NR4 and NR5) were longer than that of gold NRs with negative PT signal (NR1, NR2, and NR3). The data for all 15 gold NRs in Fig. 2b (see section 4 of ESI†) and the other measured data in Fig. 3a also support the above observation, which indicates that the measured PT signal is strongly related to the longitudinal surface plasmon resonance of the gold NR.

We also studied the influence of the polarization angle of the probe laser light on the obtained PT signal. The top panel in Fig. 2d shows the variation in the normalized PT signal Δ upon adjusting the polarization angle of the probe laser light. Here, the normalized PT signal Δ is defined as $\Delta = (I'_{iSCAT} - I_{iSCAT})/I_{ref}$, where I_{ref} is the intensity of the reflected probe light measured at the position without gold NRs (reference light). The normalized PT signal Δ oscillates as a function of the polarization angle θ. The bottom panel of Fig. 2d shows the peak intensity of the scattering spectra of gold NR4 (λ_{res} = 742 nm) recorded with an analyzer in the detection path at various angles θ. It is well known that the scattering light of the longitudinal surface plasmon resonance mode of a gold NR is mainly polarized along the long axis direction,[29] thus the in-plane orientation angle of NR4 is about 130°. Clearly, the amplitudes of the normalized PT signal Δ reach the maximum and minimum when the polarization directions of the probe laser light are parallel and perpendicular to the long axis of gold NR4, respectively, corresponding to the strongest and weakest scattered probe light from the NR4. This polarization dependence also indicates that the scattering light from gold NR plays an important role in the measured PT signal. The strong polarization dependence of the PT signal indicates that individual gold NRs can be used as orientation sensors in the resonant scattering enhanced PT microscopy.

To analyze the dependence of the normalized PT signal Δ on the longitudinal surface plasmon resonance of gold NR, we measured Δ and the corresponding scattering spectra of gold NRs covered by PVA film of different thicknesses. Δ was taken for the probe light polarized along the long axis of gold NRs. Fig. 3a and b present the distributions of the measured Δ as a function of the resonance wavelength λ_{res} for gold NRs covered by PVA film with thicknesses of 50 and 100 nm, respectively (see section 5 of ESI† for PVA thickness of 80 nm). As can be seen, the PT signal shows dramatic changes in a narrow resonance wavelength range around the wavelength of the probe light (near-resonance condition) and such changes are strongly dependent on the thickness of the PVA film. The separation of the resonance wavelength between the positive maximum and negative minimum of the PT signal in Fig. 3a is only 18 nm. The full width at the half minimum of the narrow valley in Fig. 3b is only about 15 nm, which is much smaller than the widths of the scattering spectra of gold NRs shown in Fig. 2c.

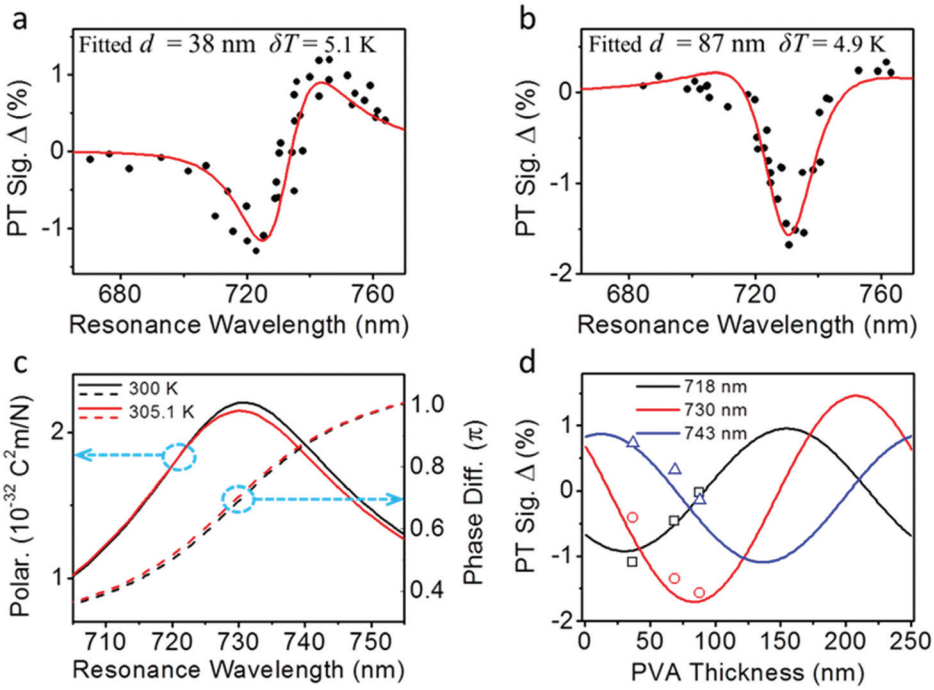

Fig. 3 (a and b) The normalized PT signal Δ as a function of the resonance wavelength λ_{res} of gold NRs. The thicknesses of the PVA films are 50 (a) and 100 (b) nm. The red solid lines represent the theoretical fits of the normalized PT signal according to eqn (2). The fitted thickness of the PVA film d and the increase in local temperature δT are provided. (c) Theoretically extracted amplitude of polarizability (polar., solid lines, left vertical axis) and phase difference between the scattering field and the reference field (phase diff., dashed lines, right vertical axis) as a function of the resonance wavelength of gold NRs in (a) with (red lines) and without (black lines) the heating beam illumination. (d) Normalized PT signal Δ of gold NRs with resonance wavelength λ_{res} of 718 (black line and hollow squares), 730 (red line and hollow circles) and 743 nm (blue line and hollow triangles) as a function of the thickness of the PVA film. The three lines are plotted according to eqn (2). The increase in the local temperature δT is 5 K. The nine hollow dots correspond to the normalized PT signal obtained from nine gold NRs measured in the experiment.

Importantly, we found that the amplitudes of the PT signal of the gold NRs in the above narrow resonance wavelength range are strongly enhanced as compared with that of gold NRs with resonance wavelength far away from the wavelength of the probe laser light (non-resonance condition, $\lambda_{res} < 700$ nm and $\lambda_{res} > 760$ nm). The maximal enhancement factor, *i.e.*, the maximal ratio of the absolute value of the PT signal at near-resonance and non-resonance conditions, was about 36 and 43 for the samples with PVA film thickness of 50 and 100 nm, respectively. This indicates that the signal-to-noise ratio of the gold NRs near-resonant with the probe light can be orders of magnitude better than the non-resonant case.

The detected intensity of iSCAT light in the absence of heating beam illumination can be expressed as follows (see section 6 of ESI†):

$$I_{iSCAT} = \left|\vec{E}_i\right|^2 \left(r^2 + |\eta\alpha|^2 + 2r\eta|\alpha|\cos\phi\right) \quad (1)$$

where $\vec{E}_i$ is the incident electric field, r is the field reflectivity at the sample interface, η takes into account the detection efficiency of the scattering field, $\alpha = |\alpha|e^{i\phi_{scat}}$ is the complex polarizability of the gold NR with information on the amplitude ($|\alpha|$) and phase-difference (ϕ_{scat}) between the scattering field and the driving field. $\phi = \phi_{scat} + \pi(1/2 - 4dn/\lambda)$ is the phase difference between the scattering field and the reference field on the detector (d and n are the thickness and refractive index of the PVA film, respectively, and λ is the wavelength of the probe light). Upon heating beam illumination, the increase in the local temperature leads to permittivity changes in the gold NR and its surrounding PVA film. The changed permittivity of PVA around each gold NR forms a small TL. The heated gold NR inside the TL can be simply treated as a core–shell NR with polarizability of $\alpha' = |\alpha'|e^{i\phi'_{scat}}$, where the shell is formed by the PVA with changed permittivity. Thus, the normalized PT signal can be given as follows:

$$\Delta = 2\frac{\eta}{r}(|\alpha'|\cos\phi' - |\alpha|\cos\phi) + \left(\frac{\eta}{r}\right)^2\left(|\alpha'|^2 - |\alpha|^2\right) \quad (2)$$

where $\phi' = \phi'_{scat} + \pi(1/2 - 4dn/\lambda)$ is the phase difference between the scattering field and the reference field with heating beam illumination. The term proportional to $(|\alpha'|^2 - |\alpha|^2)$ corresponds to the heat-induced intensity variation of pure scattering light.

We modeled the gold NR as a spheroid whose polarizability can be given in an accurate analytical formula.[30,31] The diameter of the spheroid is 20 nm and its length was used to tune the longitudinal surface plasmon resonance wavelength λ_{res}. Based on the simulated local temperature distribution around the heated gold NR (Fig. 4a and b), the heat induced "shell" around gold spheroid was fixed at 25 nm in thickness. The

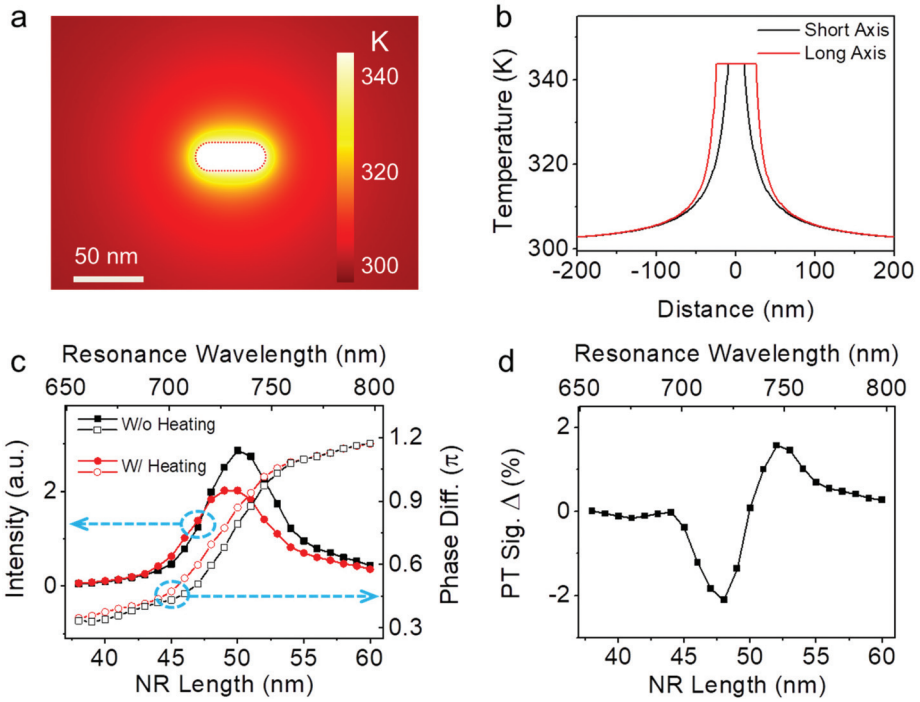

Fig. 4 (a) Temperature distribution around the gold NR on a glass substrate covered by a PVA film of 50 nm in thickness. The length and diameter of the gold NR were 50 and 20 nm, respectively. The heating beam of wavelength 532 nm was circularly polarized and the power was 2.5 mW. (b) Temperature profile along the short axis (black line) and long axis (red line) of the gold NR in (a). (c) The intensity of the extracted pure scattering light (solid dotted lines, left vertical axis) and the phase difference between the scattering field and reference field (hollow dotted lines, right vertical axis) of gold NRs without (W/o heating, black dotted lines) and with (W/heating, red dotted lines) heating beam illumination as a function of the gold NR length. The top horizontal axis shows the corresponding longitudinal surface plasmon resonance wavelength. (d) PT signal as a function of the gold NR length and the corresponding longitudinal surface plasmon resonance wavelength. The power of the heating beam is 2.5 mW.

temperature of the core–shell spheroid was assumed to be δT above room temperature (300 K). Because the absorption cross-section of gold NR at the optical excitation wavelength of the heating light (532 nm) is not size-dependent, the increase in the local temperature δT was assumed to be the same for NRs with different resonance wavelengths λ_{res} (see section 7 of ESI†). The red solid lines in Fig. 3a and b display the fits to the normalized PT signal Δ as a function of the resonance wavelength λ_{res} according to eqn (2), where η/r, d and δT were left as free-fitting parameters (see section 8 of ESI†). The experimental data and the theoretical fits in Fig. 3a and b are in good agreement. The fitted thicknesses of the PVA films are about 12–13 nm smaller than those measured in the experiment, which may be caused by the physical sizes of gold NRs. The increases in the local temperatures δT were fitted to be about 5 K. We also found that the contribution of the intensity variation of pure scattering light from gold NR to the PT signal (the term proportional to $(|\alpha'|^2 - |\alpha|^2)$ in eqn (2)) can be ignored (see section 9 of ESI†). Thus the PT signal was determined by the variation in the polarizability amplitude and the variation in the phase difference between the scattering field and the reference field, which resulted in its dependence on the resonance wavelength and PVA film thickness.

According to the fitting parameters from Fig. 3a, the black lines in Fig. 3c present the extracted amplitude of polarizability $|\alpha|$ and phase difference ϕ between the scattering field and the reference field at the probe light wavelength as a function of the resonance wavelength of gold NR without the heating beam illumination. The amplitude of polarizability is maximal for the gold NR with a resonance wavelength λ_{res} of 730 nm, in accordance with the wavelength of the probe light. Similar to a mechanical oscillator driven by a harmonic force, where a pronounced phase difference of π between the in-phase and out-of-phase oscillation around the eigenfrequency is introduced, the scattering field from the gold NR experienced a transition from the in-phase ($\phi_{scat} = 0$) to the out-of-phase ($\phi_{scat} = \pi$) oscillation, with respect to the driving field, when the resonance wavelength λ_{res} scanned across the wavelength of the probe light (see section 10 of ESI†). The offset between ϕ and ϕ_{scat} was determined by the thickness of the PVA film in the form of $\pi(1/2 - 4dn/\lambda)$. The red solid and red dashed lines of Fig. 3c show the extracted $|\alpha'|$ and ϕ' as a function of the resonance wavelength of gold NR upon heating beam illumination. As can be seen, the polarizability and phase differences were shifted to the left and the maximum amplitude of polarizability decreased because the increase in the local temperature around the gold NR led to the permittivity changes in the gold NR and the surrounding PVA medium. Clearly, the heat-induced variation in the polarizability and the phase difference is more obvious for gold NR near-resonant with the probe

light, as compared with the non-resonant gold NR (see section 11 of ESI†), which resulted in the enhanced PT signal in the narrow resonance wavelength range around the wavelength of the probe light. Based on our calculations, the polarizability of the heated gold NR in the TL (heat-induced "shell") near the longitudinal surface plasmon resonance conditions was nearly the same as that of the gold NR embedded in the uniform medium with the permittivity of the TL (see section 12 of ESI†). This means that the PT signal of the gold NR near-resonant with the probe light was mainly caused by the heat-induced variation in the polarizability of the gold NR, and the scattering field from the TL can be ignored. The variation in the polarizability of the gold NR was caused by the heat-induced variation in the permittivity of PVA and gold, and the red-shift in the resonance wavelength (see section 13 of ESI†).

Fig. 3d shows the normalized PT signal Δ as a function of the thickness of the PVA film plotted according to eqn (2) for gold NRs with different resonance wavelengths. Clearly, the PT signal oscillates with the increased thickness of the PVA film, which linearly changes the phase difference between the scattering field and the reference field. The maximum amplitude of the PT signal was obtained for gold NR with a resonance wavelength of 730 nm, the same as the wavelength of the probe laser light (see section 14 of ESI†). The experimental results for PVA thicknesses of 50, 80, and 100 nm are also plotted in Fig. 3d, which agree well with the theoretical results.

In order to confirm the experimental results and verify the theoretical treatment above, we performed numerical simulations by using finite-element method-based commercial software COMSOL Multiphysics to study the PT signal caused by the heating beam illumination (see section 15 of the ESI† for more simulation details). Without loss of generality, the PVA film in our simulation was 50 nm in thickness. The diameter of the NR was 20 nm. Fig. 4a shows the simulated temperature distribution around the gold NR of 50 nm in length. The simulation yielded an increase in the local temperature of about 40 K at the incident power of 2.5 mW. The temperature was uniform on the NR and decayed rapidly away from the NR surface in the surrounding medium with a characteristic length of about 25 nm (see Fig. 4b and section 16 of the ESI†). The simulated temperature on the gold NR was about 12 K above room temperature at the incident power of 0.72 mW (see section 16 of the ESI†), which was higher than the fitting result of about 5 K in Fig. 3. We attributed this difference to the quickly decreasing temperature around the NR surface, while the temperature of the TL shell was assumed to be the same as that of the gold NR in our theoretical treatment.

Fig. 4c shows the intensity of the extracted pure scattering field and the phase difference between the scattering field and the reference field as a function of the length of the NR (and the corresponding resonance wavelength without the heating beam illumination) with and without the heating beam illumination. The intensity of the pure scattering field without heating beam illumination is maximal for gold NR with resonance wavelength the same as the probe light wavelength of 730 nm, corresponding to the maximum polarizability amplitude. The simulated phase difference ϕ of the gold NR (without heating beam illumination) in-phase and out-of-phase with the incident probe light are 0.32π and 1.17π, respectively, which is consistent with our fitting result of 0.28π and 1.13π. Upon heating beam illumination, the intensity of the pure scattering field and the phase difference were left-shifted and the maximal intensity was reduced (red curves in Fig. 4c), which agrees with our experimental fitting results in Fig. 3c. The simulated PT signal was negative and positive for gold NR with lengths shorter and longer than the critical length of about 50 nm (corresponding to λ_{res} of 733 nm), respectively (Fig. 4d). Compared with the gold NR non-resonant with the probe light (λ_{res} < 695 nm and λ_{res} > 770 nm), the maximum enhancement factor of the amplitude of the PT signal was more than 42 for gold NR near-resonant with the probe light. All these features of the simulated PT signal are consistent with our experimental and theoretical fitting results shown in Fig. 3a.

The dramatic variation in the PT signal in a narrow resonance wavelength range could enable the identification and characterization of gold NRs with very high precision. The PT signal of gold NR near-resonant with the probe light is also very sensitive to the variation in the local refractive index. Our calculation shows that the 0.1 percent variation in the local refractive index could result in the change in the PT signal as high as 40 percent, which is over 10 times more sensitive than the scattering and absorption cross-section-based gold NR sensors (see section 17 of ESI†). Such high sensitivity could enable the direct identification of binding and unbinding events of a single protein, which would greatly expand the resonant PT microscopy to the fields of analytical chemistry and nanobiology. Compared with the maximal enhancement factor of 43 measured in the experiment, the theoretical calculation shows that the PT signal of gold NRs (20 nm in diameter) near-resonant with the probe laser light can be enhanced by as much as 500 times that of the completely non-resonant gold NRs (λ_{res} < 650 nm). Compared with the previous non-resonant PT techniques, the strongly enhanced PT signal here could enable the wide field and video-rate imaging of nanoparticles by using a commercial camera without the restriction of the scanning stage and lock-in amplifier with long integration time.

Conclusion

In summary, we developed a novel strategy to enhance the PT signal by using resonant scattering as demonstrated by gold NR with a tunable longitudinal surface plasmon mode. It was observed in the experiment that the PT signal of the gold NR near-resonant with the probe light was strongly enhanced, as high as 43 times, compared with that of gold NR with the resonance wavelength being tens of nanometers away from the probe light wavelength. Theoretical analysis showed that the enhanced PT signal was mainly caused by the heat-induced variation of the polarizability of the gold NR. These results can

promote the development of resonant scattering-enhanced PT microscopy with much higher sensitivity, and better functionality and flexibility.

Conflicts of interest

There are no conflicts to declare.

Acknowledgements

Q.L. and Z.S. contributed equally to this work. This work was supported by National Natural Science Foundation of China (Grants 61675070, 61378082, 11704133, and 11774413), the Foundation for Distinguished Young Talents in Higher Education of Guangdong (Grant 2016KQNCX031), and the Ministry of Science and Technology of China (Grant 2015CB932400).

References

1 R. W. Taylor, R. G. Mahmoodabadi, V. Rauschenberger, A. Giessl, A. Schambony and V. Sandoghdar, *Nat. Photonics*, 2019, **13**, 480–487.
2 G. Young, N. Hundt, D. Cole, A. Fineberg, J. Andrecka, A. Tyler, A. Olerinyova, A. Ansari, E. G. Marklund, M. P. Collier, S. A. Chandler, O. Tkachenko, J. Allen, M. Crispin, N. Billington, Y. Takagi, J. R. Sellers, C. Eichmann, P. Selenko, L. Frey, R. Riek, M. R. Galpin, W. B. Struwe, J. L. P. Benesch and P. Kukura, *Science*, 2018, **360**, 423–427.
3 G. Young and P. Kukura, *Annu. Rev. Phys. Chem.*, 2019, **70**, 301–322.
4 J. O. Arroyo and P. Kukura, *Phys. Chem. Chem. Phys.*, 2012, **14**, 15625–15636.
5 K. Lindfors, T. Kalkbrenner, P. Stoller and V. Sandoghdar, *Phys. Rev. Lett.*, 2004, **93**, 037401.
6 J. Kirstein, B. Platschek, C. Jung, R. Brown, T. Bein and C. Bräuchle, *Nat. Mater.*, 2007, **6**, 303.
7 E. Betzig, G. H. Patterson, R. Sougrat, O. W. Lindwasser, S. Olenych, J. S. Bonifacino, M. W. Davidson, J. Lippincott-Schwartz and H. F. Hess, *Science*, 2006, **313**, 1642–1645.
8 C. Sönnichsen, T. Franzl, T. Wilk, G. von Plessen, J. Feldmann, O. Wilson and P. Mulvaney, *Phys. Rev. Lett.*, 2002, **88**, 077402.
9 R. M. Dickson, A. B. Cubitt, R. Y. Tsien and W. E. Moerner, *Nature*, 1997, **388**, 355.
10 Q. Li, X. J. Chen, Y. Xu, S. Lan, H. Y. Liu, Q. F. Dai and L. J. Wu, *J. Phys. Chem. C*, 2010, **114**, 13427–13432.
11 R. J. Ober, S. Ram and E. S. Ward, *Biophys. J.*, 2004, **86**, 1185–1200.
12 D. Boyer, P. Tamarat, A. Maali, B. Lounis and M. Orrit, *Science*, 2002, **297**, 1160–1163.
13 L. Cognet, C. Tardin, D. Boyer, D. Choquet, P. Tamarat and B. Lounis, *Proc. Natl. Acad. Sci. U. S. A.*, 2003, **100**, 11350–11355.
14 A. Gaiduk, P. V. Ruijgrok, M. Yorulmaz and M. Orrit, *Chem. Sci.*, 2010, **1**, 343.
15 P. Vermeulen, L. Cognet and B. Lounis, *J. Microsc.*, 2014, **254**, 115–121.
16 M. Selmke, M. Braun and F. Cichos, *ACS Nano*, 2012, **6**, 2741–2749.
17 S. Berciaud, L. Cognet, G. A. Blab and B. Lounis, *Phys. Rev. Lett.*, 2004, **93**, 257402.
18 W. S. Chang, J. W. Ha, L. S. Slaughter and S. Link, *Proc. Natl. Acad. Sci. U. S. A.*, 2010, **107**, 2781–2786.
19 C. Pache, N. L. Bocchio, A. Bouwens, M. Villiger, C. Berclaz, J. Goulley, M. I. Gibson, C. Santschi and T. Lasser, *Opt. Express*, 2012, **20**, 21385–21399.
20 M. Yorulmaz, S. Khatua, P. Zijlstra, A. Gaiduk and M. Orrit, *Nano Lett.*, 2012, **12**, 4385–4391.
21 E. S. Shibu, N. Varkentina, L. Cognet and B. Lounis, *Adv. Sci.*, 2017, **4**, 1600280.
22 U. Bhattacharjee, C. A. West, S. A. Hosseini Jebeli, H. J. Goldwyn, X. T. Kong, Z. W. Hu, E. K. Beutler, W. S. Chang, K. A. Willets, S. Link and D. J. Masiello, *ACS Nano*, 2019, **13**, 9655–9663.
23 S. Berciaud, L. Cognet and B. Lounis, *Nano Lett.*, 2005, **5**, 2160–2163.
24 S. Berciaud, L. Cognet and B. Lounis, *Phys. Rev. Lett.*, 2008, **101**, 077402.
25 S. Berciaud, L. Cognet, P. Poulin, R. B. Weisman and B. Lounis, *Nano Lett.*, 2007, **7**, 1203–1207.
26 A. Gaiduk, M. Yorulmaz, P. V. Ruijgrok and M. Orrit, *Science*, 2010, **330**, 353–356.
27 I. Ament, J. Prasad, A. Henkel, S. Schmachtel and C. Sönnichsen, *Nano Lett.*, 2012, **12**, 1092–1095.
28 P. Zijlstra, P. M. R. Paulo and M. Orrit, *Nat. Nanotechnol.*, 2012, **7**, 379–382.
29 C. Sönnichsen and A. P. Alivisatos, *Nano Lett.*, 2005, **5**, 301–304.
30 C. F. Bohren and D. R. Huffman, *Absorption and Scattering of Light by Small Particles*, John Wiley & Sons. Inc., New York, 1998.
31 S. Link, M. B. Mohamed and M. A. El-Sayed, *J. Phys. Chem. B*, 1999, **103**, 3073–3077.